LASER INTERFEROMETER GRAVITATIONAL WAVE OBSERVATORY
- LIGO -
CALIFORNIA INSTITUTE OF TECHNOLOGY
MASSACHUSETTS INSTITUTE OF TECHNOLOGY

Technical Note	**LIGO-T2100198–v1**	2021/07/14

Back-action evasion for PT-symmetric interferometer

Student: Kagan Yanik
Mentors: Rana Adhikari, Yanbei Chen, Xiang Li, Shruti Jose Maliakal

California Institute of Technology
LIGO Project, MS 18-34
Pasadena, CA 91125
Phone (626) 395-2129
Fax (626) 304-9834
E-mail: info@ligo.caltech.edu

Massachusetts Institute of Technology
LIGO Project, Room NW22-295
Cambridge, MA 02139
Phone (617) 253-4824
Fax (617) 253-7014
E-mail: info@ligo.mit.edu

LIGO Hanford Observatory
Route 10, Mile Marker 2
Richland, WA 99352
Phone (509) 372-8106
Fax (509) 372-8137
E-mail: info@ligo.caltech.edu

LIGO Livingston Observatory
19100 LIGO Lane
Livingston, LA 70754
Phone (225) 686-3100
Fax (225) 686-7189
E-mail: info@ligo.caltech.edu

http://www.ligo.caltech.edu/

1 Introduction/Background

1.1 General Intro

Future gravitational and astrophysical research calls for the broadband and high-frequency sensitivity of gravitational wave detectors. Conventional resonant detectors are subject to bandwidth-peak sensitivity trade-off. The idea to circumvent this limitation, i.e. to improve the bandwidth without sacrificing the peak sensitivity, is called White Light Cavity (WLC). The PT-symmetric interferometer with coherent quantum feedback [1] is a stable realization of WLC (which is called sWLC for short), compared with the direct attachment of a filter cavity with anomalous dispersion [2] (uWLC for short). However, the original proposal [1] hasn't considered the back-action noise caused by the radiation pressure on the test mass.

In this project, we work with the PT symmetric interferometer. We aim to explore a more complete PT-symmetric structure to improve the low-frequency noise spectrum by back-action evasion with an effective negative mass. The effective negative mass will be possibly achieved using parametric amplification and optical damping formed by multiple additional pumpings. and hence, have a larger bandwidth with sacrificing less of the sensitivity than we would for a conventional trade-off between the bandwidth and sensitivity.

In Gravitational Wave detection, we mainly use laser interferometers, especially Michelson-type interferometers with suspended mirrors (suspended mirrors behave as free mass above the resonance frequency [7]). Gravitational waves incident on an interferometer exert a signal force on the interferometer, which causes optical displacement between the end mirrors of the interferometer. The dimensionless parameter describing the amplitude of this displacement is called strain (h) and the optical displacement (path length change) is expressed by

$$\delta x = Lh \tag{1}$$

where L is the arm length [7]. In our project, we use an arm cavity for this purpose and express it with the differential mode $\hat{a}$ since the output of the cavity depends on the differential phase between the two arms of the cavity.

1.2 Bandwidth Sensitivity Trade-off

In a setup with an arm cavity and a strain signal that comes to detector, we see a trade-off between the bandwidth and the peak sensitivity of the strain noise at the detector as a result of Energetic Quantum Limit (EQL) which is represented by the inequality [1]

$$\int_0^{+\infty} d\Omega/(2\pi) S_h^{-1}(\Omega) \leq \Delta\mathcal{E}^2/(4\hbar)^2 \tag{2}$$

If we want a larger bandwidth, we would have to have a flatter peak sensitivity and for a sharper peak sensitivity, we would have a smaller bandwidth for the strain noise being detected, hence the trade-off.

1.3 Anomalous Dispersion

To deal with the restraints of the EQL, we need to create anomalous dispersion [2]. The arm cavity from the initial setup has phase delay. We attach a filter cavity (which has a movable mirror with mechanical oscillation frequency ω_m), to the arm cavity, with phase advance to compensate for the phase delay. From the phase point of view, the two cavities can be thought as the time reversal of each other. As a result, we have a zero and constant phase for much larger bandwidth for light circulating inside the two cavities. This can be achieved by anomalous dispersion, which is a parametric interaction and helps us realize the white light cavity. Assuming that the arm cavity with the phase delay has resonant frequency ω_0, we pump the filter cavity with the detuned light at the frequency $\omega_0 + \omega_m$ [2]. As a result of this parametric interaction, we get to have a larger bandwidth, at the same level of sensitivity as before. However, this parametric interaction is unstable.

1.4 PT-symmetric Interferometer

Even though the unstable White Light Cavity (uWLC) can overcome the bandwidth sensitivity trade-off, we seek to stabilize the system, because unstability brings technical complications with the feedback control of the system.

To stabilize the system we will use a coherent quantum feedback with PT-symmetry where we place the detector at the end of the filter cavity to get the readout. It can be seen from FIG. 1 that in the unstable case (uWLC) modes $\hat{b}$ and $\hat{c}$ are at the filter cavity and attached to the arm cavity (mode $\hat{a}$) from which we get the readout. On the other hand, for sWLC, we get the readout from the filter cavity (mode $\hat{b}$) which also satisfies the PT-symmetry.

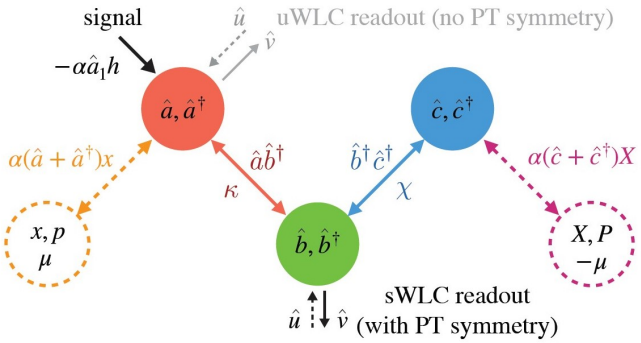

Figure 1: The stable White Light Cavity (sWLC) scheme [1]. The arm cavity has mode $\hat{a}$, the filter cavity has mode $\hat{c}$ and the detector has mode $\hat{b}$. Mode $\hat{a}$ couples to mode $\hat{b}$ with a coupling rate κ and mode $\hat{c}$ couples to mode $\hat{b}$ with coupling rate χ. Mode $\hat{b}$ is coupled to stable WLC (sWLC) readout. This system is PT symmetric when χ=κ. $\hat{u}$ is the input vacuum noise (quantum noise) and $\hat{v}$ is the output field.

Both for the uWLC and sWLC, the interaction Hamiltonian is expressed as [1]

$$\hat{V}_{\text{int}} = i\hbar\kappa(\hat{a}\hat{b}^\dagger - \hat{a}^\dagger\hat{b}) + i\hbar\chi(\hat{b}^\dagger\hat{c}^\dagger - \hat{b}\hat{c}). \tag{3}$$

1.5 Coherent Quantum Feedback

In the unstable White Light Cavity system (uWLC), discussed in the anomalous dispersion section, the filter cavity attached to the arm cavity acts as a coherent quantum feedback controller.

Looking at the equations of motion for modes, $\hat{a}$, $\hat{b}$, and $\hat{c}$ [1]

$$\dot{\hat{a}} = -\kappa\hat{b} + i\alpha h \tag{4}$$

$$\dot{\hat{c}}^\dagger = \chi\hat{b} \tag{5}$$

$$\dot{\hat{b}} = -\gamma_R\hat{b} + \kappa\hat{a} + \chi\hat{c}^\dagger + \sqrt{2\gamma_R}\hat{u} \tag{6}$$

and ignoring the signal part of mode $\hat{a}$ (iαh), we see that in the PT symmetric case, the equations of motion for mode $\hat{a}$ and $\hat{c}^\dagger$ are equal and opposite. Therefore, the following expression

$$\frac{d}{dt}(\chi\hat{a} + \kappa\hat{c}^\dagger) = i\chi\alpha h \tag{7}$$

is exclusively dependent on the signal [1]. In this equation, we obtain an internal mode (the expression inside the time derivative) which responds to the signal only, providing a coherent quantum feedback inside the system (between the modes $\hat{a}$ and $\hat{c}$). The internal mode is also a part of the readout mode ($\hat{b}$), but it is not influenced by the noise from the readout.

In this project we aim to use the coherent quantum feedback to stabilize our system.

1.6 Backaction

Backaction is due to the photons imparting momentum to the mirrors in the system. We can also call this radiation pressure. Moreover, the inserted momentum will influence the position measurement at later times. The backaction noise will increase when we increase the pumping power of the laser. In our project, we observe backaction when the strong field interacts with the test mass μ with mode (x,p) attached to mode $\hat{a}$. Due to backaction, both the conventional and any WLC noise spectra have a tail at low frequencies [1] where radiation pressure noise is effective, which can be seen in FIG. 2.

2 Objectives

2.1 Backaction Evasion

In this project, our objective is to add back-action evasion module to realize the full PT-symmetric structure of FIG. 1 which has not been described in prior work [1]. To preserve the PT-symmetry structure of the system, (since $\hat{a}$ and $\hat{c}$ are PT-symmetric) we aim to attach another mode (X,P) with negative mass $-\mu$ to mode $\hat{c}$. The P-symmetry is done by attaching (X,P) to $\hat{c}$ and T-symmetry is preserved by the negative mass since $\dot{X} = \frac{P}{-\mu}$. Conserving the PT-symmetry of the system causes backaction evasion, which flattens the tails of uWLC and sWLC noise spectrum curves at low frequencies.

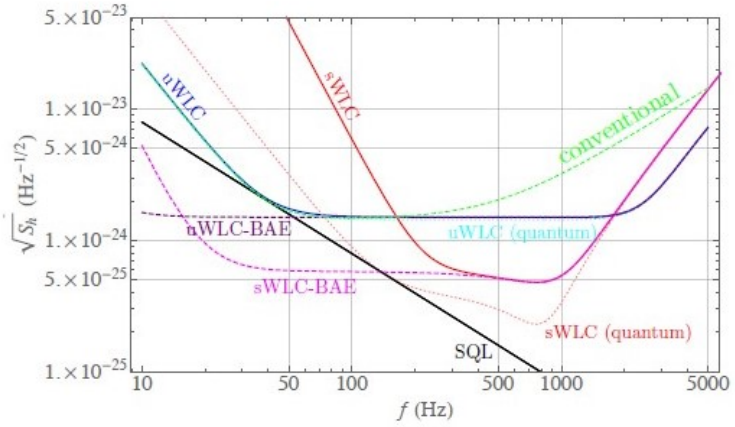

Figure 2: GW noise spectra for sWLC and uWLC both with and without backaction evasion (BAE) [1]. We can see that the tails of uWLC and sWLC at low frequencies have been flattened more due to backaction evasion.

3 Approach

3.1 Negative Mass

The complete description of the system includes the optomechanical interaction between test mass (x, p) and the cavity mode $\hat{a}$. The total Hamiltonian is given by

$$\hat{H} = \alpha(\hat{a} + \hat{a}^\dagger)x + \frac{\hat{p}^2}{2\mu} + \hat{V}_{\rm int}, \tag{8}$$

where μ is the reduced mass of the cavity mirrors, and $\hat{V}_{\rm int}$ is given in Eq. (3) where the PT-symmetry was initially constructed by adding a filter cavity to the arm cavity. Considering the interaction between mode $\hat{a}$ and the test mass (x, p), the PT-symmetry is no longer reserved. To restore the PT-symmetry of the system, we need to add a negative mass counterpart and attach it to mode $\hat{c}$:

$$\hat{V}_{\rm aux} = \alpha(\hat{c} + \hat{c}^\dagger)X + \frac{\hat{P}^2}{-2\mu}. \tag{9}$$

Attaching (X, P) to mode $\hat{c}$will conserve the P-symmetry, while the negative mass will conserve the time reversal symmetry.

To implement this negative mass in our system, we propose to add an optomechanical auxiliary mode ($\hat{d}$, $\hat{d}^\dagger$), which is expressed by the Hamiltonian

$$\hat{V}_{\rm aux} = \alpha X_{\rm ZPF}(\hat{c}\hat{d} + \hat{c}\hat{d}^\dagger + \hat{c}^\dagger\hat{d} + \hat{c}^\dagger\hat{d}^\dagger) + \frac{1}{-2\mu}\left(\frac{\hbar}{2iX_{\rm ZPF}}\right)^2(\hat{d}^2 - \hat{d}\hat{d}^\dagger - \hat{d}^\dagger\hat{d} + \hat{d}^{\dagger 2}) \tag{10}$$

where $\hat{c}^\dagger\hat{d}^\dagger$ is the non-degenerate squeezing generator which can be generated by blue tuned pumping, $\hat{c}\hat{d}^\dagger$ is the beam splitter generated by red detuned pumping, and $\hat{d}^2 + \hat{d}^{\dagger 2}$ are the squeezing terms.

Besides this optomechanical system, other realizations such as a nonlinear crystal realization can potentially achieve similar results.

4 Progress

4.1 Coherent amplification of sensitivity by sWLC

Over the first three weeks of the research we first analyzed the sWLC with modes $\hat{a}, \hat{b}, \hat{c}$, without the test mass $(\hat{x}, \hat{p})$ attached to mode $\hat{a}$. This means that the system has no back-action since we did not put the position $(\hat{x})$ of the end mirror as a dynamical quantity. In this case, we derived the total Hamiltonian of the system as

$$\hat{H}_{total} = -\alpha \frac{(\hat{a} + \hat{a}^\dagger)}{\sqrt{2}} h + i\hbar\kappa(\hat{a}\hat{b}^\dagger - \hat{a}^\dagger\hat{b}) + i\hbar\chi(\hat{b}^\dagger\hat{c}^\dagger - \hat{b}\hat{c}) \tag{11}$$

where the first term of the equation is the Hamiltonian for the coupling between the mode $\hat{a}$ and the signal from the GW. The other two terms are the interaction Hamiltonian due to coupling between modes $\hat{a}$-$\hat{b}$ and modes $\hat{b}$-$\hat{c}$. Based on this Hamiltonian we derived the equations of motion for the modes $\hat{a}, \hat{b}, \hat{c}$ in the Heisenberg picture, then applied Fourier transform to get the equations in the frequency domain and then added dissipation for losses:

$$-i\Omega\hat{a} = -\kappa\hat{b} + i\alpha h \tag{12}$$

$$-i\Omega\hat{c}^\dagger = \chi\hat{b} - \gamma_m\hat{c}^\dagger + \sqrt{2\gamma_m}\hat{w} \tag{13}$$

$$-i\Omega\hat{b} = -\gamma_R\hat{b} + \kappa\hat{a} + \chi\hat{c}^\dagger + \sqrt{2\gamma_R}\hat{u} \tag{14}$$

where $\hat{w}$ is the thermal noise and γ_m is the dissipation rate (which does not come directly from the Hamiltonian) since we also taken into account the thermal noise at $\hat{c}^\dagger$ which decays to a thermal bath [4]. The output field for any case [1] is expressed as

$$\hat{v} = \hat{u} - \sqrt{2\gamma_R}\hat{b} \tag{15}$$

where $\hat{u}$ is the quantum noise and γ_R is the readout rate. From the equations of motion that we derived earlier, using Solve[] function in Mathematica, we obtain the expression

$$\hat{v} = C1h + C2\hat{u} + C3\hat{w} \tag{16}$$

where C1, C2, and C3 are the coefficients of the signal, quantum noise and thermal noise respectively. The spectral density of the noise in the system is found by

$$S = \langle\hat{v}^\dagger\hat{v}\rangle. \tag{17}$$

Assuming that the noise sources are uncorrelated, we obtained the following expressions for each noise source's h-normalized spectral density:

$$S_u^h = \left|\frac{C2}{C1}\right|^2, \tag{18}$$

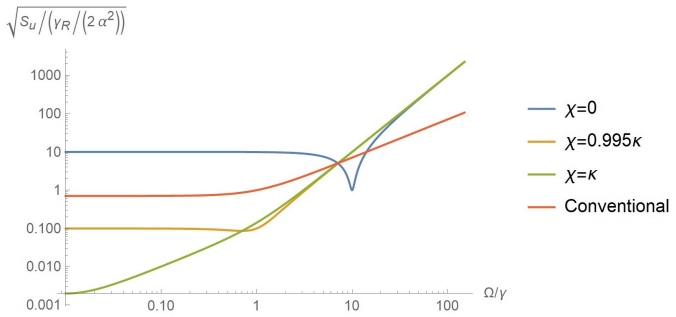

Figure 3: Normalized spectral density for the quantum noise in sWLC (for three different χ values) and single-cavity (conventional) detector for $\gamma_R = 1 rad Hz, \gamma_m = 0.000001 rad Hz, \kappa = 10\gamma_R$.

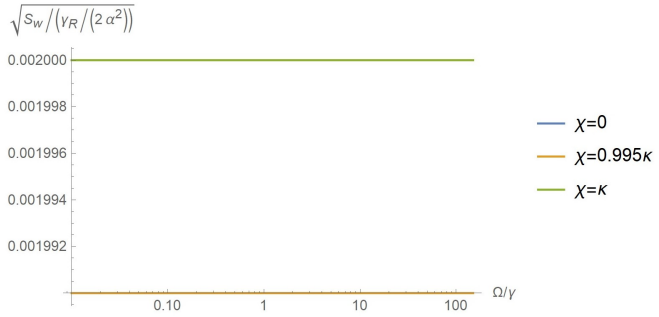

Figure 4: Normalized spectral density for the thermal noise in sWLC (for three different χ values) for $\gamma_R = 1 rad Hz, \gamma_m = 0.000001 rad Hz, \kappa = 10\gamma_R$.

$$S_w^h = \left|\frac{C3}{C1}\right|^2. \tag{19}$$

As a result, we simulated the normalized spectral density plots for the quantum noise and thermal noise for $\chi = 0, 0.995\kappa, \kappa$ in Mathematica.

In FIG. 3, we have recreated FIG.4 from the broadband sensitivity paper [1]. We see that in the PT-symmetry case ($\chi = \kappa$) the quantum noise is the lowest of all the other parameters at lower frequencies. Hence, PT-symmetry improves the sensitivity of the sWLC at lower frequencies. Close to PT-symmetry threshold ($\chi = 0.995\kappa$) the quantum noise is almost stable at lower frequencies, yet lower than the conventional detector. When there is no $\hat{b}-\hat{c}$ coupling, the quantum noise of sWLC is the highest compared to all other parameters. Moreover, we see an additional peak in quantum noise when there is no $\hat{b}-\hat{c}$ coupling. When we have all three modes noise from $\hat{b}$ goes into modes $\hat{a}$ and $\hat{c}$ simultaneously. However, when we delete $\hat{c}$ from the system, we obtain a feedback loop only between $\hat{a}$ and $\hat{b}$ which works like a detuned interferometer whose resonance depends on κ. This extra resonance causes the peak in our plot which increases the sensitivity.

We can see that PT-symmetry is effective in reducing the quantum noise at lower frequencies while it is not effective at higher frequencies since PT-symmetric interferometer targets sensitivity near DC which corresponds to the lower frequencies. As we can see from Eq.7, PT-symmetry creates a coherent kernel between $\hat{a}$ and $\hat{c}$ such that the specific combination of these modes will respond infinitely to signal. The outcome of the infinite signal integral only leaves the signal from lower frequencies which have near DC behavior.

In FIG. 4, we see that there is no thermal noise when there is no PT-symmetry since there is no $\hat{b}-\hat{c}$ coupling and $\hat{c}$ is the only source of thermal noise. PT-symmetry has the highest thermal noise since it has the strongest $\hat{b}-\hat{c}$ coupling. The thermal noise is mostly constant, mainly because the thermal decay rate is low compared to the readout rate.

4.1.1 GW Noise Spectra for sWLC with Backaction

We now attach a test mass μ $(\hat{x}, \hat{p})$ to mode $\hat{a}$. This coupling causes radiation pressure (backaction) noise and is effective at lower frequencies as opposed to the shot noise which is effective at higher frequencies. As mentioned in the Approach section, we aim to cancel the backaction noise via backaction evasion by coupling a negative mass μ_c $(\hat{X}, \hat{P})$ to mode $\hat{c}$. Hence, we derived the Hamiltonian for backaction evasion as

$$\hat{H}_{total} = i\hbar\kappa(\hat{a}\hat{b}^\dagger - \hat{a}^\dagger\hat{b}) + i\hbar\chi(\hat{b}^\dagger\hat{c}^\dagger - \hat{b}\hat{c}) + \alpha(\hat{a}+\hat{a}^\dagger)(\hat{x} - Lh) + \alpha(\hat{c}+\hat{c}^\dagger)\hat{X}. \tag{20}$$

Based on this Hamiltonian, we derived the equations of motion for modes $\hat{a}, \hat{b}, \hat{c}^\dagger, \hat{x}, \hat{p}, \hat{X}, \hat{P}$ in amplitude-phase quadrature where amplitude is denoted by 1 and phase is denoted by 2.

$$-i\Omega\hat{a}_1 = -\kappa\hat{b}_1, \tag{21}$$

$$-i\Omega\hat{a}_2 = -\kappa\hat{b}_2 + \alpha(\hat{x} - Lh), \tag{22}$$

$$-i\Omega\hat{b}_1 = -\gamma_R\hat{b}_1 + \kappa\hat{a}_1 + \chi\hat{c}_1 + \sqrt{2\gamma_R}\hat{u}_1, \tag{23}$$

$$-i\Omega\hat{b}_2 = -\gamma_R\hat{b}_2 + \kappa\hat{a}_2 - \chi\hat{c}_1 + \sqrt{2\gamma_R}\hat{u}_2, \tag{24}$$

$$-i\Omega\hat{c}_1 = \chi\hat{b}_1 - \gamma_m\hat{c}_1 + \sqrt{2\gamma_m}\hat{w}_1, \tag{25}$$

$$-i\Omega\hat{c}_2 = -\chi\hat{b}_2 + \alpha X - \gamma_m\hat{c}_2 + \sqrt{2\gamma_m}\hat{w}_2, \tag{26}$$

$$-i\Omega\hat{x} = \frac{\hat{p}}{\mu}, \tag{27}$$

$$-i\Omega\hat{p} = \sqrt{2}\alpha\hat{a}_1, \tag{28}$$

$$-i\Omega\hat{X} = \frac{\hat{P}}{\mu_c}, \tag{29}$$

$$-i\Omega\hat{p} = \sqrt{2}\alpha\hat{c}_1, \tag{30}$$

In these equations modes $(\hat{x}, \hat{p})$ and $(\hat{X}, \hat{P})$ provide feedback loops since $\hat{x}$ and $\hat{X}$ obtain information from the amplitude quadratures of $\hat{a}$ and $\hat{c}$ respectively and give information to the phase quadratures of $\hat{a}$ and $\hat{c}$ respectively. We observed four different cases: sWLC with BAE and thermal noise (case 1), with BAE but without thermal noise (case 2), without BAE but with thermal noise (case 3), without BAE or thermal noise (case 4). The equations we derived above are for case 1. For case 2 we use the condition $\gamma_m = 0$. For case 3, omit the negative mass modes $(\hat{X}, \hat{P})$, and for case 4, we use the conditions from case 2 and 3 both. Evaluating the output field in phase quadrature, we derive the expressions (in Mathematica) for h-normalized noise spectral densities using the same method in the previous section and plot the results in Mathematica. We also scale the spectral density for each thermal noise by the population expressed by $(k_B T)/(\hbar\omega_m)$ where k_B is the Boltzmann constant and T is the temperature of the thermal bath mode $\hat{c}$ is coupled to.

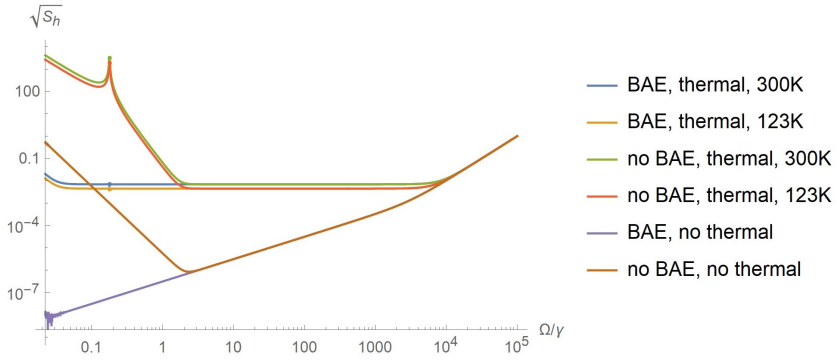

Figure 5: Normalized noise spectral density for the four cases mentioned previously for the parameters $\alpha = 1, \gamma_R = 2\pi(500)Hz, \gamma_m = 0.000001Hz$ or $0Hz$ (depending on the case), $\kappa = \chi = 10\gamma_R, L = 4000m, -\mu_c = \mu = 50000g, T = 300K$ or $123K, \omega_m = 10kHz$.

We show that BAE (due to negative mass) cancels the backaction noise since the spectral densities for the cases with BAE are lower than the others at lower frequencies. Since thermal noise is also dominant at lower frequencies, the case with BAE and thermal noise has higher noise at lower frequencies than the case with BAE but no thermal noise. When the thermal noise is omitted, the spectral densities increase linearly in mid-frequency range and quadratically in high frequencies (in log-log scale). When there is thermal noise, the spectral density is almost constant at mid-frequency range and then increases quadratically

and same as no-thermal-noise plots (in log-log scale). Thermal noise gets bigger as thermal bath temperature increases and the highest noise comes from no BAE with thermal noise.

We also observed a sudden peak at the case without BAE but with thermal noise at lower frequency range. This is because we obtain a pole for the sWLC near 0.06 Hz and we believe that it is because we introduced a thermal decay rate γ_m which shifts the pole from 0 Hz to 0.06 Hz. As the thermal decay rate gets lower,the peak's location get closer to 0 Hz. We also notice fluctuations for the case with BAE and no thermal noise at lower frequencies. These fluctuations result from numerical errors in simulation.

During our process of deriving the equations and plotting the spectral densities in Mathematica, we have run into many errors. To solve these errors, we did dimensional analysis on the derived expressions (coefficients, spectral densities, etc.), chose the right scales to show the spectral density plots, chose the right/reasonable values for the parameters, and check the terms and their physical meanings of the terms in derivations.

5 Future Directions

For the next step of our project, we aim to implement a physical system for the negative mass and characterize it with an optomechanical mode $(\hat{d}, \hat{d}^\dagger)$. So far we have done readings and discussed about the realization of a negative mass in physical systems such as a multiatom spin ensemble [5, 6] or a mechanical oscillator [5] entangled with an auxiliary mode.

References

[1] Li, Xiang, et al, *Broadband sensitivity improvement via coherent quantum feedback with PT symmetry*. arXiv preprint arXiv:2012.00836 (2020).

[2] Miao, Haixing, et al, *Enhancing the Bandwidth of Gravitational-Wave Detectors with Unstable Optomechanical Filters*. Phys. Rev. Lett. 115, 211104

[3] Chen, Yanbei, *Macroscopic quantum mechanics: theory and experimental concepts of optomechanics*. Journal of Physics B: Atomic, Molecular and Optical Physics 46.10 (2013): 104001.

[4] Li, Xiang, et al, *Supplementary Material for Broadband sensitivity improvement via coherent quantum feedback with PT symmetry*.

[5] Tsang, Mankei and Caves, Carlton M. *Evading quantum mechanics*. arXiv preprint arXiv:1203.2317 (2012).

[6] Khalili, F. Ya. and Polzik, E. S. *Overcoming the Standard Quantum Limit in Gravitational Wave Detectors Using Spin Systems with a Negative Effective Mass*. Phys. Rev. Lett. 121, 031101

[7] Arai, Koji, *Gravitational wave detection with laser interferometers*. LIGO SURF 2021 Lecture Presentation.